AWARD NUMBER:	W81XWH-20-1-0888
TITLE:	New Antibody-Cytokine Fusion Proteins for the Therapy of Neuroblastoma
PRINCIPAL INVESTIGATOR:	Dr. Rosa Nguyen
CONTRACTING ORGANIZATION:	The Geneva Foundation 917 Pacific Ave, Suite 600 Tacoma, WA 98402-4437
REPORT DATE:	January 2023
TYPE OF REPORT:	Final
PREPARED FOR:	U.S. Army Medical Research and Development Command Fort Detrick, Maryland 21702-5012
DISTRIBUTION STATEMENT:	Approved for Public Release; Distribution Unlimited

REPORT DOCUMENTATION PAGE

Form Approved
OMB No. 0704-0188

1. REPORT DATE	2. REPORT TYPE	3. DATES COVERED
January 2023	Final report	15SEPT2020 14SEPT2022

4. TITLE AND SUBTITLE

New Antibody-Cytokine Fusion Proteins for the Therapy of Neuroblastoma

5a. CONTRACT NUMBER

5b. GRANT NUMBER
W81XWH-20-1-0888

5c. PROGRAM ELEMENT NUMBER

6. AUTHOR(S)

Dr. Rosa Nguyen
Hongharosa.nguyen@nih.gov

5d. PROJECT NUMBER

5e. TASK NUMBER

5f. WORK UNIT NUMBER

7. PERFORMING ORGANIZATION NAME(S) AND ADDRESS(ES)

The Geneva Foundation
917 Pacific Avenue. Suite 600
Tacoma, WA 98402

8. PERFORMING ORGANIZATION REPORT NUMBER

9. SPONSORING / MONITORING AGENCY NAME(S) AND ADDRESS(ES)

U.S. Army Medical Research and Development Command
Fort Detrick, Maryland 21702-5012

10. SPONSOR/MONITOR'S ACRONYM(S)

11. SPONSOR/MONITOR'S REPORT NUMBER(S)

12. DISTRIBUTION / AVAILABILITY STATEMENT

Approved for Public Release; Distribution Unlimited

13. SUPPLEMENTARY NOTES

14. ABSTRACT

To improve immunotherapy for neuroblastoma, an anti-disialoganglioside (GD2) antibody and interleukin (IL)-2 fusion protein was generated (hu14.18-IL-2) that achieved tumor regression in 16-22% of patients enrolled in phase II clinical trials. However, more than 90% of participating children experienced toxicity, and bulky tumors did not respond. I recently demonstrated that substituting IL-15 for IL-2 in a current neuroblastoma immunotherapy regimen resulted in elevated levels of cytotoxicity in mice with bulky tumors, conceivably by promoting differentiation of tumor-infiltrating NK cells and upregulation of Gzmd. IL-21, a pleiotropic cytokine that also activates NK cells, has not been broadly studied in neuroblastoma. Herein, I propose to engineer and test new antibody-cytokine fusion proteins for the treatment of neuroblastoma. Objectives/hypothesis: The objective of this grant proposal is to determine the effectiveness of two novel antibody-cytokine fusion proteins, aGD2-IL-15 and aGD2-IL-21, and compare them with hu14.18-IL-2. I hypothesize that aGD2-IL-15 and aGD2-IL-21 can cause equivalent or higher tumor regression than hu14.18- IL-2, presumably due to cytokine-specific phenotypic and transcriptomic changes in tumor-infiltrating lymphocytes (TILs).

15. SUBJECT TERMS
Cancer, Oncology, Neuroblastoma

16. SECURITY CLASSIFICATION OF:			17. LIMITATION OF ABSTRACT	18. NUMBER OF PAGES	19a. NAME OF RESPONSIBLE PERSON
a. REPORT	b. ABSTRACT	c. THIS PAGE			19b. TELEPHONE NUMBER *(include area code)*
Unclassified	Unclassified	Unclassified	Unclassified	20	USAMRDC

Standard Form 298 (Rev. 8-98)
Prescribed by ANSI Std. Z39.18

TABLE OF CONTENTS

1. INTRODUCTION:

Neuroblastoma, the most common extracranial solid malignancy of childhood, accounts for 12% of all cancer deaths in pediatrics, highlighting the need for novel therapies. Immunotherapy with a monoclonal anti-GD2 antibody and interleukin (IL)-2 has significantly improved the survival in these patients when given in a state of minimal residual disease (MRD). However, IL-2 is associated with significant toxicities. In efforts to limit the toxic side effects and enhance anti-tumor efficacy, an anti-GD2 antibody-IL-2 conjugate was generated (hu14.18-IL-2). In a human phase II study, 5 of 31 patients (16%) with MRD achieved a complete response with hu14.18-IL-2. However, over 90% of the patients experienced grade 3 or 4 adverse events, highlighting the limitations of this therapy. I recently demonstrated that substituting IL-15 for IL-2 resulted in elevated levels of antibody-mediated cytotoxicity (ADCC) in vivo. IL-21, a cytokine that also activates NK cells, has not been broadly studied in neuroblastoma. Herein, I propose to engineer and test new antibody-cytokine fusion proteins for the treatment of neuroblastoma in preclinical model systems.

2. KEYWORDS:

Neuroblastoma, antibody, cytokines, interleukin, natural killer cells, pediatric cancer.

3. ACCOMPLISHMENTS:

What were the major goals of the project?

Research-Specific Tasks:

Specific Aim 1: Determine if ADCC induced by aGD2-IL15 and aGD2-IL21 is equivalent or superior to hu14.18-IL-2.			
Major Task 2: Produce aGD2-IL15 and aGD2-IL-21	**Months**	**NCI**	**Completed?**
Subtask 2.1: Obtain transfected clone Cell lines used: CHO cells [ATCC]	1-2	Dr. Nguyen	**Yes**
Subtask 2.2: Purify and validate recombinant antibody-cytokine fusion proteins	2-10	Dr. Nguyen	
Major Task 3: Test anti-tumor effect of aGD2-IL15 and aGD2-IL-21	**Months**	**NCI**	**Completed?**
Subtask 3.1: Test aGD2-IL15/IL21 in vitro Cell lines used: NSX-2 [Dr. Paul Sondel lab], SJNBL046_X and SJNBL012407_X1 [CSTN]	10-12	Dr. Nguyen	**Yes**
Subtask 3.2: Perform pharmacokinetic studies with aGD2-IL15/IL21 in vivo Cell lines used: NSX-2 [Dr. Paul Sondel lab], SJNBL046_X and SJNBL012407_X1 [CSTN] Animals used: 30 CD1-*Foxn1*^{nu} mice [Charles River laboratories], 30 A/J mice [Jackson laboratories]	10-12	Dr. Nguyen	**Yes**
Subtask 3.3: Test ADCC by aGD2-IL15/IL21 in vivo Cell lines used: NSX-2 [Dr. Paul Sondel lab], SJNBL046_X and SJNBL012407_X1 [CSTN] Animals used: 140 CD1-*Foxn1*^{nu} mice [Charles River laboratories], 110 A/J mice [Jackson laboratories]	12-18	Dr. Nguyen	**Yes**

Specific Aim 2: Investigate the relative contribution of NK cells to ADCC induced by aGD2-IL-15 and aGD2-IL-21.			
Major Task 4: Perform in vivo NK cell depletion	**Months**	**NCI**	**Completed?**

Subtask 4.1: Perform NK cell depletion in vivo and perform in vivo testing with aGD2-IL15/IL21	12-18	Dr. Nguyen	**Not done**

This Major Task was not performed because our study revealed that T cells and macrophages were the response-driving cell populations and not NK cells.

Specific Aim 3: Investigate the transcriptional and phenotypic changes in TILs in the presence of aGD2-IL-15 and aGD2-IL-21.			
Major Task 5: Submit samples for single-cell RNA-seq	**Months**	**NCI**	**Completed?**
Subtask 5.1: Submit TILs samples for single-cell RNA-seq	12-18	Dr. Nguyen	**Yes**
Subtask 5.2: Perform in silico analysis of single-cell RNA-seq data	18-24	Dr. Nguyen	**Yes**

What was accomplished under these goals?

We attached the publication that resulted from this work. It was published in Clinical Cancer Research (impact factor: 13.8) as a cover story. **Nguyen R, Zhang X, Sun M, Abbas S, Seibert C, Kelly MC, Shern JF, Thiele CJ. Anti-GD2 Antibodies Conjugated to IL15 and IL21 Mediate Potent Antitumor Cytotoxicity against Neuroblastoma. Clin Cancer Res. 2022 Sep 1;28(17):3785-3796. doi: 10.1158/1078-0432.CCR-22-0717. PMID: 35802683**

What opportunities for training and professional development did the project provide?
How were the results disseminated to communities of interest?

Training-Specific Tasks:

Major Task 1: Training and educational development in neuroblastoma cancer research	**Months**	**NCI**	**Completed?**
Subtask 1.1: Attend a cancer immunotherapy workshop	6-12	Dr. Nguyen	**Yes**
Subtask 1.2: Present research at the monthly departmental meetings	12-24	Dr. Nguyen	**Yes**

Subtask 1.3: Present research at the Advances in Neuroblastoma Research meeting 2020	6-12	Dr. Nguyen	**Not done**
Subtask 1.4: Draft manuscript and prepare for publication	18-24	Dr. Nguyen	**Yes**

Subtask 1.3 was not done because the meeting has been repeatedly postponed due to the COVID-19 pandemic.

How were the results disseminated to communities of interest?
The results are part of my NCI Annual Report. The Pediatric Oncology Branch and the CCR News announced the study on their Twitter account.

4. IMPACT:

What was the impact on the development of the principal discipline(s) of the project?

The novel ACCs have the potential to be the next generation of antibodies for clinical testing in neuroblastoma. The experiments that I have designed and conducted have the purpose to provide a preclinical rationale to move these inventions into the clinic and translate them into a treatment regimen that can benefit children with neuroblastoma. The ACCs are a novel line of therapy; thus, the first-in-human administration of these ACCs would yield a new understanding of the immunologic mechanisms of these immunotherapies. Their applicability could be expanded to other $GD2^+$ cancers, such as melanoma.

What was the impact on other disciplines?
As mentioned above, we are testing these antibodies in neuroblastoma. However, the use of these molecules could be potentially expanded to other cancer entities that express GD2.

What was the impact on technology transfer?
Nothing to Report.

What was the impact on society beyond science and technology?
Nothing to Report.

5. CHANGES/PROBLEMS:

Changes in approach and reasons for change
Nothing to Report.

Actual or anticipated problems or delays and actions or plans to resolve them:
Nothing to Report.

Changes that had a significant impact on expenditures
Nothing to Report.

Significant changes in use or care of human subjects, vertebrate animals, biohazards, and/or select agents:

Significant changes in use or care of human subjects:
Not applicable.

Significant changes in use or care of vertebrate animals:
Nothing to Report.

Significant changes in use of biohazards and/or select agents:
Nothing to Report.

6. PRODUCTS:

Publications, conference papers, and presentations

Journal publications:
Nguyen R and Thiele CJ. Immunotherapy approaches targeting neuroblastoma. Curr Opin Pediatr. 2021;33(1):19-25. Published; acknowledgement of federal support: yes.

Nguyen R, Zhang X, Sun M, Abbas S, Seibert C, Kelly MC, Shern JF, Thiele CJ. Anti-GD2 Antibodies Conjugated to IL15 and IL21 Mediate Potent Antitumor Cytotoxicity against Neuroblastoma. Clin Cancer Res. 2022 Sep 1;28(17):3785-3796. doi: 10.1158/1078-0432.CCR-22-0717. PMID: 35802683. Published; acknowledgement of federal support: yes.

Books or other non-periodical, one-time publications:
Nothing to report.

Other publications, conference papers, and presentations:
Nothing to report.

Website(s) or other Internet site(s):
Nothing to report.

Technologies or techniques:
Nothing to report.

Inventions, patent applications, and/or licenses:
Nothing to report.

Other Products:
Nothing to report.

7. PARTICIPANTS & OTHER COLLABORATING ORGANIZATIONS:

No change.

Has there been a change in the active other support of the PD/PI(s) or senior/key personnel since the last reporting period?
Nothing to Report.

What other organizations were involved as partners?
Nothing to Report.

8. SPECIAL REPORTING REQUIREMENTS:

Nothing to report.

9. APPENDICES:

Attached:

- Publication
- Award chart

Anti-GD2 Antibodies Conjugated to IL15 and IL21 Mediate Potent Antitumor Cytotoxicity against Neuroblastoma

Rosa Nguyen[1], Xiyuan Zhang[1], Ming Sun[1], Shahroze Abbas[1], Charlie Seibert[2], Michael C. Kelly[2], Jack F. Shern[1], and Carol J. Thiele[1]

ABSTRACT

Purpose: Half of the patients with high-risk neuroblastoma who receive GD2-targeted mAb do not achieve long-term remissions. Recently, the antibody hu14.18 has been linked to IL2 (hu14.18-IL2) to enhance its efficacy and shown promising preclinical and clinical activity. We developed two new immunocytokines (IC) by linking two other γ_c cytokines, IL15 and IL21, to hu14.18. The purpose of this study was to compare hu14.18-IL15 and -IL21 with hu14.18-IL2 in their ability to induce antibody-dependent cell-mediated cytotoxicity (ADCC) against neuroblastoma.

Experimental Design: We assessed ADCC of hu14.18-IL15 and -IL2 (human cytokines, cross-reactive to mouse) against $GD2^{low}$ and $GD2^{high}$ neuroblastoma cell lines *in vitro*. T-cell–deficient mice with orthotopic patient-derived xenografts (PDX) and immunocompetent mice with transplantable orthotopic neuroblastoma were used to test all three ICs, including hu14.18-IL21 (murine IL21, not cross-reactive to human). Mechanistic studies were performed using single-cell RNA-sequencing (scRNA-seq).

Results: hu14.18-IL15 and hu14.18-IL2 mediated equivalent *in vitro* ADCC by human NK cells. When combined with chemotherapy, all three ICs similarly controlled the growth of PDXs in nude mice with murine NK effector cells. However, hu14.18-IL15 and -IL21 outperformed hu14.18-IL2 in immunocompetent mice with syngeneic neuroblastoma, inducing complete tumor regressions and extending survival. scRNA-seq data revealed an increase in $CD8^+$ T cells and M1 tumor-associated macrophages and decreased regulatory T cells and myeloid-derived suppressor cells in the tumor microenvironment.

Conclusions: Hu14.18-IL15 and Hu14.18-IL21 exhibit robust preclinical activity, warranting further consideration for clinical testing in patients with GD2-expressing neuroblastoma.

Introduction

mAb therapy targeting GD2 is part of the standard of care for patients with high-risk neuroblastoma (1). However, 50% of treated patients still do not achieve long-term remissions (2). To enhance antitumor efficacy, an antibody–cytokine conjugate (immunocytokine, IC) was developed by linking IL2 to the COOH terminus of a humanized anti-GD2 antibody (hu14.18-IL2; refs. 3, 4). Although hu14.18-IL2 eradicated minimal residual disease in mice and patients, those with bulky tumors did not respond, highlighting the limitations of this therapy (5–7).

Soluble IL2 was originally part of the immunotherapy regimen to treat neuroblastoma but has been removed because its therapeutic benefit was called into question owing to severe toxicities associated with higher doses and unestablished efficacy at lower doses (8). IL2 belongs to the γ_c family of cytokines and induces pro-immune effects by engaging the IL2 receptor γ (IL2Rγ) and cytokine-specific receptor subunits (IL2Rα and IL2/15Rβ), which are expressed on various effector cells of antibody-dependent cell-mediated cytotoxicity (ADCC; ref. 9). IL15 and IL21, other members of this family, have overlapping biologic effects with IL2, but their therapeutic use in neuroblastoma has been underappreciated until recently. For example, we and others have shown that IL15/IL15Rα complexes enhance ADCC against neuroblastoma to a greater extent than soluble IL2 (10, 11). However, it is unknown whether ICs linked with IL15 and IL21 can effectively target neuroblastoma and how their activity compares with hu14.18-IL2.

In this study, we found that hu14.18-IL15 induced equivalent ADCC against GD2-expressing neuroblastoma as hu14.18-IL2 *in vitro* with human NK cells serving as effector cells. Equivalency was also observed in T-cell–depleted patient-derived xenograft (PDX) models *in vivo* with NK cells as primary effector cells. However, in fully immunocompetent syngeneic mouse models with orthotopic neuroblastoma, hu14.18-IL15 and -IL21 outperformed hu14.18-IL2. Single-cell RNA sequencing (scRNA-seq) data revealed significant differences in the remodeling of the tumor microenvironment (TME), potentially overcoming immunosuppressive mechanisms. In summary, this work demonstrates the importance of IL15 and IL21 γ_c family of cytokines as adjunct agents for mAb therapy in neuroblastoma.

Materials and Methods

Cell lines

NXS-2-$GD2^+$ (*Mycn*-wild-type, WT) was the kind gift of Dr. Paul Sondel (University of Wisconsin). The PDXs SJNBL012407_X1 and SJNBL046_X (both *MYCN*-amplified) were provided by the Children's Solid Tumor Network. IMR-5, IMR-32, KCNR, SKNBE2C (all *MYCN*-amplified), SKNFI, SH-SY5Y, and SKNAS (latter three *MYCN*-WT) were retrieved from the laboratory repository. All cells tested negative for *Mycoplasma* (Mycoalert, Lonza) before use. Their identity was confirmed by short-tandem repeat DNA profiling. Thawed cells were used within 3 months.

Stable luciferase (ffLUC)–GFP-expressing cells were generated by lentiviral transduction. Neuroblastoma cell lines were selected with

[1]Pediatric Oncology Branch, Center for Cancer Research, National Cancer Institute, National Institutes of Health, Bethesda, Maryland. [2]Center for Cancer Research Single Cell Analysis Facility CCR, Cancer Research Technology Program, Frederick National Laboratory, Bethesda, Maryland.

Corresponding Author: Rosa Nguyen, National Cancer Institute, 10 Center Drive, Building 10, Room 1W-5816, Bethesda, MD 20892. Phone: 443-902-3243; Fax: 301-451-7052; E-mail: hongharosa.nguyen@nih.gov

Clin Cancer Res 2022;28:3785–96

doi: 10.1158/1078-0432.CCR-22-0717

Translational Relevance

An anti-GD2 antibody linked to IL2 (hu14.18-IL2) has shown promising preclinical and clinical activity against neuroblastoma. Nevertheless, the overall therapeutic benefit of IL2 has remained questionable owing to severe toxicities associated with higher doses and unestablished efficacy at lower doses. We developed two new antibody–cytokine conjugates by linking two other γ_c cytokines, IL15 and IL21, to hu14.18. In immunocompetent models of neuroblastoma, we demonstrate superior antibody-dependent cell-mediated cytotoxicity of hu14.18-IL15 and -IL21 compared with hu14.18-IL2. Single-cell RNA-sequencing studies indicate that hu14.18-IL15 and -IL21 may mechanistically act by increasing activated $CD8^+$ T cells and M1 tumor-associated macrophages and limiting the recruitment of T regulatory cells and myeloid-derived suppressor cells to the tumor microenvironment. Altogether, hu14.18-IL15 and hu14.18-IL21 exhibit robust preclinical activity, warranting further consideration for clinical testing in patients with GD2-expressing neuroblastoma.

0.5 μg/mL of puromycin (Thermo Fisher Scientific) and cryopreserved with >60% enrichment for transduced cells. PDX cells were transduced with freshly prepared concentrated lentivirus particles and grown for 24 hours in full RPMI medium and on Matrigel-coated plates (Corning Inc.) before injection into mice. After one passage in mice, cells were cryopreserved.

Human NK cells

Fresh human NK cells were isolated from buffy coats of healthy volunteer donors (NIH Blood Bank) via magnetic bead negative selection (Stem Cell Technology). >95% purity of $CD45^+$ $CD56^+$ $CD3^-$ NK cells was deemed acceptable for further experiments (Supplementary Fig. S1).

Generation of ICs

The humanized anti-GD2 antibody hu14.18, an IgG1 isotype antibody, which contains a WT F_c, was conjugated at the COOH terminus via a $(G_4S)_3$ linker to human IL15 (cross-reactive to mouse) or murine IL21 (not cross-reactive to human) to obtain research-grade protein for experimental use (Creative Biolabs; Supplementary Fig. S2). Hu14.18-IL2 (human IL2, which is cross-reactive to mouse) was obtained from the Biological Resources Branch at the Frederick National Laboratory (BRB Frederick). We confirmed intact conjugation of the antibody and respective cytokines using a sandwich ELISA assay with the anti-idiotypic antibody 1A7 (BRB Frederick) as capture antibody as previously described (12). We also confirmed detection of antibody and cytokines in the tumors and serum at 48 hours (Supplementary Fig. S3).

In vitro activation assay

Freshly isolated human NK cells were incubated in descending dilutions of ICs or soluble human IL15 or IL2 (BRB, Frederick). To quantify the level of cellular activation, CD69 expression was measured by flow cytometry after 24 hours of co-culture.

In vitro ADCC assay

NK cells and ffLUC-expressing tumor cells were co-cultured in the presence or absence of ICs (1 μg/mL) at varying effector-to-tumor (E:T) ratios as previously described (13). After 24 hours, the specific lysis of the tumor cells was measured using the ONE-Glo Luciferase Assay System (Promega).

In vitro rechallenge assay

One day before the assay, IMR-5-ffLUC-GFP cells were added to flat-bottom 96-well plates at a density of 10,000 cells per well. The next day, human NK cells and ICs (1 μg/mL) were added at an E:T ratio of 5:1. Cell confluence was monitored every four hours using the Incucyte system (Sartorius) by recording the area emitting fluorescent GFP signal. Every 24 hours thereafter, 10,000 IMR-5-ffLUC-GFP cells were added to each well to rechallenge the NK cells. The experiment was terminated when controls reached confluence.

Mice

For neuroblastoma PDX studies, 4- to 6-week-old female athymic nude mice were obtained from the NCI CCR Animal Resource Program/NCI Biological Testing Branch. For syngeneic studies, 4- to 6-week-old female A/J mice were purchased from The Jackson Laboratory. All animal studies were approved by the Institutional Animal Care and Use Committee of the National Cancer Institute (protocol number: PB-023).

Bioluminescence imaging

Tumor-bearing mice were injected with d-luciferin potassium salt (150 mg/kg, intraperitoneal), anesthetized with isoflurane, and imaged on an IVIS Lumina XR System (PerkinElmer) 5 minutes after d-luciferin injection (1 minute acquisition time). Region of interest analysis was performed using the Living Image software (PerkinElmer; version 4.3.1).

In vivo humanized chemoantibody therapy model

Athymic nude mice lack T cells and have decreased levels but functional monocytes and NK cells, thus enabling the engraftment of PDX tumors and the study of ADCC as previously shown (10). In this model, chemotherapy comprised intraperitoneal injections of irinotecan (1.6 mg/kg) and oral temozolomide (16.5 mg/kg) for 5 days. Immunotherapy was given to respective mice one week after chemotherapy as five daily intravenous injections (50 μg per dose) as previously described (10). Mice received two treatment courses with each course lasting 3 weeks (third week of rest), emulating clinical regimens (14, 15). First, PDX cells were implanted orthotopically (2.5×10^5) into athymic nude mice (16). Typically, three weeks after tumor implantation surgery, animals meeting enrollment criteria with a bioluminescence imaging (BLI; $>10^7$), were randomized to receive either (i) vehicle, (ii) daily chemotherapy, (iii) chemotherapy followed by hu14.18-IL2, (iv) chemotherapy followed by hu14.18-IL15, or (v) chemotherapy followed by hu14.18-IL21. The experiment was terminated on day 65 after tumor injection. BLI signals did not correlate with tumor burden in the PDX model, particularly in mice with large tumors. Therefore, we recorded tumor weights (primary endpoint) and the occurrence of metastases (secondary endpoint) to determine the efficacy of the treatments.

In vivo syngeneic antibody therapy model

A/J mice underwent orthotopic injection of NXS-2-ffLUC-GFP cells (5×10^5; ref. 3). Eight days later, when they established a defined BLI signal ($>10^6$), mice received daily injections of ICs (25 μg per dose) for 5 consecutive days intravenous. The tumor weight was determined on day 30 after tumor implantation or survival of treated mice was monitored until day 100. Survival endpoints were death, >20% weight loss from baseline, or severe moribund status.

Flow cytometry

Samples were stained using 10^6 cells. Gates were drawn with fluorescence-minus-one controls. Compensations and voltages were set with single-color controls. The following antibodies were used for detection of surface epitopes: CD45 (clone 30-F11), CD3 (OKT3), CD4 (RM4–4), CD8 (53–6.7), F4/80 (BM8), CD25 (3C7), CD49b (DX5), CD45 (HI30), CD69 (FN50), CD56 (5.1H11), TIGIT (A15153G), and GD2 (14.G2a; all BioLegend). Intracellular molecules were detected with Foxp3 (MF14), IFNγ (XMG1.2), and Perforin (S16009A) antibody. The PE Phycoerythrin Fluorescence Quantitation Kit (BD Biosciences) was used to determine the density of GD2 expression in tumor cells. Data were collected on a Fortessa LSR machine and analyzed in FlowJo v10.

Cytokine bead assay

Cytokine bead assays were conducted to quantitate the secreted cytokines in the supernatant of co-cultures following the manufacturer's instructions (BioLegend).

scRNA-seq

A/J mice were injected orthotopically with NXS-2 cells (5×10^5). Three weeks later, mice were randomly stratified into four different groups to receive (i) Vehicle, (ii) hu14.18-IL2, (iii) hu14.18-IL15, (iv) hu14.18-IL21. ICs were administered intravenously as one dose of 25 μg. About 48 hours later, tumors were processed into single-cell suspensions and enriched via CD45 magnetic bead–positive selection (Stem Cell Technologies). The viability of samples was confirmed to be >80% before further processing. Three individual mouse samples per treatment group were pooled. About 10,000 cells from each treatment group were loaded with the goal of capturing 6,000 cells using the 10X Genomics 3′ v3.1 chemistry. We followed the manufacturer's instructions for library generation. The cDNA libraries were sequenced on the NextSeq2000 with a target depth of approximately 50,000 reads per cell.

Biocomputational analysis

The 10X Genomics "cellranger" pipeline was applied to align reads to the mouse mm10 genome with default settings and to generate a single-cell gene expression matrix. Ambient RNA was removed using the SoupX algorithm by setting the contamination rate at 30% (17). Doublets were detected by the scrublet package and removed for the downstream analysis in Seurat (v4.0.1; refs. 18, 19). Cells with low (<50 genes) and aberrantly high numbers of genes (>7,000 genes) were removed. Cells that contained more than 10% mitochondria genes were removed. Sample integration across the treatment groups was performed using the standard anchor-based workflow in Seurat. For initial clustering and annotation, we applied the KNN graph based on the weighted RNA similarities, to calculate the Jaccard index (neighborhood overlap) between every pair of cells with a high resolution and merging of clusters. Results were presented on Uniform Manifold Approximation and Projection plots for visualization using the Seurat package. Tumor cells were identified by the green fluorescent protein sequence. $CD45^+$ immune cells were annotated using canonical gene markers. Lymphoid and myeloid cells were separated and reclustered to obtain more refined cell clusters. Differential gene expression was calculated for all pairs of clusters and therapy groups.

Statistical analysis

Two groups were compared using the Student *t* test (normally distributed data) or Mann–Whitney *U* test (skewed data). For experiments with more than two groups, the statistical significance was assessed using a one-way ANOVA (normally distributed data) followed by Tukey *post hoc* comparison tests or a one-way ANOVA on ranks (skewed data) followed by the Dunn test. For survival analysis, Kaplan–Meier curves were generated, and a two-sided log-rank test was performed to examine the differences between survival curves with significance level adjusted for multiple comparisons with the Bonferroni method. All experiments were repeated at least once.

Data availability

Materials and data are available from the corresponding author upon reasonable written request. The scRNA-seq data were deposited in GEO (GSE206628).

Results

Hu14.18-IL15 and hu14.18-IL2 demonstrate equivalent ADCC against neuroblastoma *in vitro*

To measure the activating effects of the ICs on human NK cells, we co-cultured NK cells with descending concentrations of hu14.18-IL15 and hu14.18-IL2. Soluble IL2 and IL15 served as positive controls, supplementing the media at concentrations commonly used to expand NK cells in culture (13, 20). After 24 hours, we analyzed the cells for the expression of CD69 as an activation marker. Both ICs were able to activate NK cells in a dose-dependent manner compared with controls (**Fig. 1A**). Slightly higher CD69 levels were noted with hu14.18-IL2 than -IL15. The IC-mediated activation was accompanied by secretion of the effector molecules perforin and granzyme A into the culture supernatant at 48 hours (**Fig. 1B**).

We went on to evaluate ADCC against the $GD2^{high}$ neuroblastoma cell lines, IMR-32, IMR-5, and KCNR. The cytotoxic capacity of NK cells was significantly increased at various E:T ratios by the addition of either one of the ICs (**Fig. 1C**). We then extended our testing to six neuroblastoma cell lines with $GD2^{high}$ or $GD2^{low}$ expression (**Fig. 1D**). ICs increased NK cell-mediated tumor lysis of $GD2^{high}$ cell lines, whereas lytic levels of $GD2^{low}$ neuroblastoma were similar with or without ICs (**Fig. 1E**). These findings demonstrate that hu14.18-IL15 and hu14.18-IL2 both activate NK cells and significantly enhance their cytotoxic potential against $GD2^{high}$ but not $GD2^{low}$ neuroblastoma *in vitro*.

NK cells maintain their cytolytic capacity with ICs during tumor rechallenge

To assess NK cell function during continuous tumor exposure, we conducted a tumor rechallenge experiment. Human NK cells were co-cultured with GFP-expressing IMR-5 cells ± hu14.18 or ICs at an E:T ratio of 5:1. IMR-5 is very suitable for this imaging-based assay, given that the morphology of the cell line is flat and the GFP signal strong (**Fig. 2A**). Every 24 hours thereafter, the starting number of tumor cells was added to each well, and cytolysis was monitored by quantifying the GFP^+ area. The efficacy by which NK cells eliminated tumor diverged after the second tumor rechallenge (**Fig. 2B**). Tumor confluence continued to increase with NK cells alone, whereas hu14.18 allowed NK cells to restrict tumor growth but rendered them unable to eliminate tumor cells. NK cells harnessed with ICs effectively lysed tumor cells with each consecutive rechallenge. After the fifth tumor rechallenge, residual NK cells had attained a predominantly $CD56^{bright}$ status and expressed high levels of CD69, suggestive of NK cell activation (**Fig. 2C**). In contrast, hu14.18 without

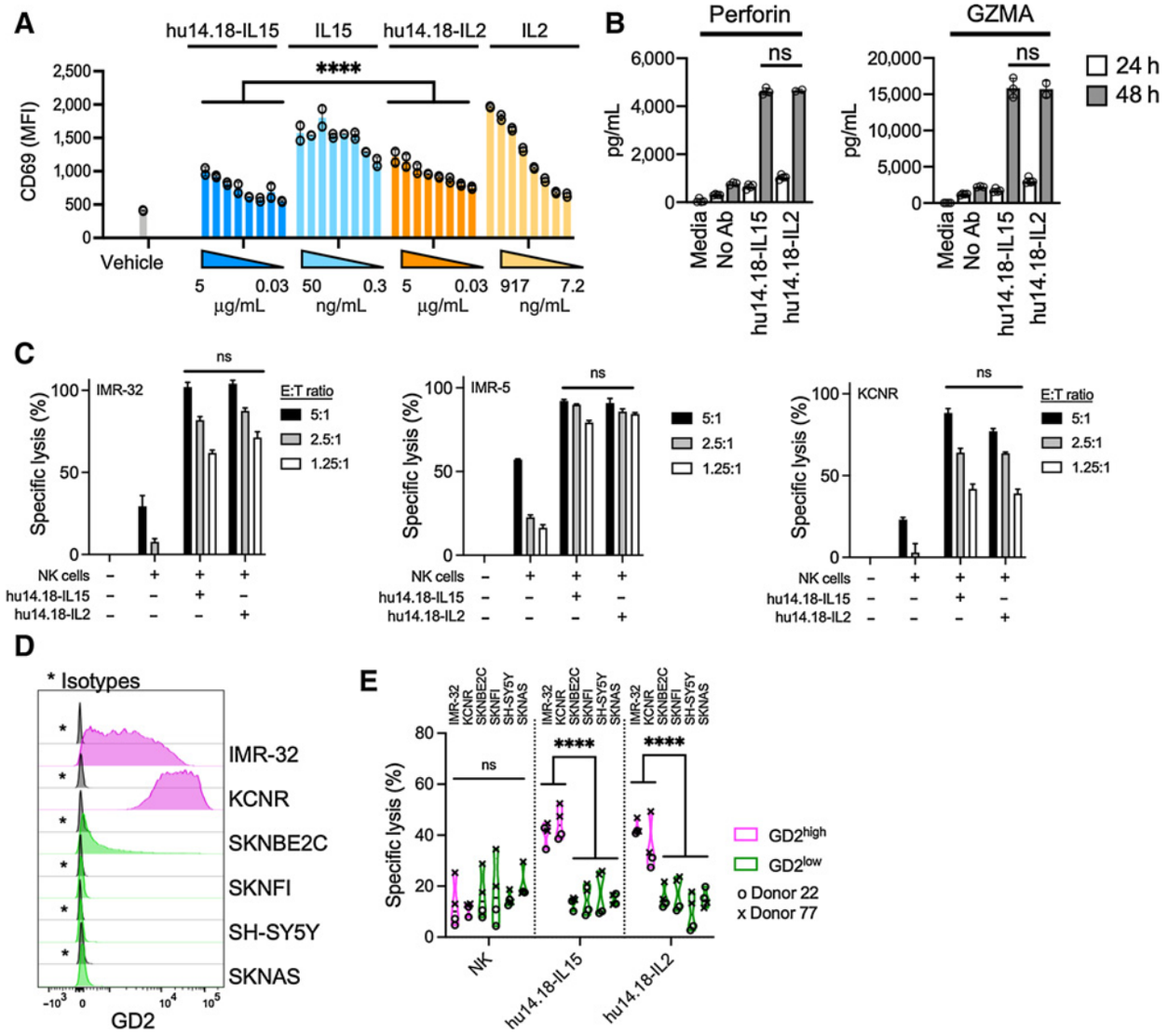

Figure 1.

Hu14.18-IL15 and hu14.18-IL2 have equivalent ADCC against neuroblastoma *in vitro*. **A,** CD69 expression of human NK cells to detect NK cell activation; paired *t* test, ****, $P < 0.0001$. **B,** Soluble perforin and granzyme A levels in the supernatant of NK cell cultures ± ICs; paired *t* test; ns, nonsignificant. **C,** 24-hour ADCC of IMR-32 IMR-5, and KCNR by human NK cells plated at varying E:T ratios ± ICs; paired *t* test; ns, nonsignificant. **D,** GD2 levels of six neuroblastoma cell lines; *, isotype controls. **E,** ADCC of NK cells against GD2^{high} and GD2^{low} neuroblastoma cells plated at an E:T ratio of 5:1 and IC concentration of 1 µg/mL; unpaired *t* test, ****, $P < 0.0001$. One of two experimental replicates using two different donors is shown for (**A–C**).

human cytokines was associated with a CD56^{dim} phenotype. The expression of TIGIT, a marker of functional NK cell exhaustion, was higher in hu14.18-IL2– than hu14.18-IL15–treated cells and altogether elevated when compared with hu14.18 and NK cells alone. The supernatant after the final rechallenge showed significantly higher levels of granulysin, granzyme B, perforin, sFASL, and IFNγ with hu14.18-IL2 than hu14.18-IL15. NK cells expanded in the presence of IL2-conjugated antibodies (**Fig. 2D** and **E**). Our findings demonstrate that both ICs can maintain the cytolytic capacity of NK cells against neuroblastoma. Hu14.18-IL2 led to more robust NK cell expansion and cytokine secretion compared with hu14.18-IL15 but upregulated TIGIT, suggestive of early signs of functional exhaustion.

ICs combined with chemotherapy control neuroblastoma PDXs in T-cell–deficient mouse models

We have previously demonstrated that athymic nude mice can engraft with orthotopic neuroblastoma PDXs and serve as a preclinical model for chemo-immunotherapy testing (10). Like our previous experience, we noted again that ICs alone do not induce ADCC in mice with bulky tumor (Supplementary Fig. S4), consistent with clinical observations that ICs have better activity in patients with minimal residual disease than bulky tumor (5, 21). Hence, we compared the antitumor activity of the ICs combined with chemotherapy to chemotherapy with irinotecan and temozolomide alone (**Fig. 3A**) using two *MYCN*-amplified GD2^{high} PDXs (**Fig. 3B**). ICs combined with chemotherapy mediated complete tumor regression in two

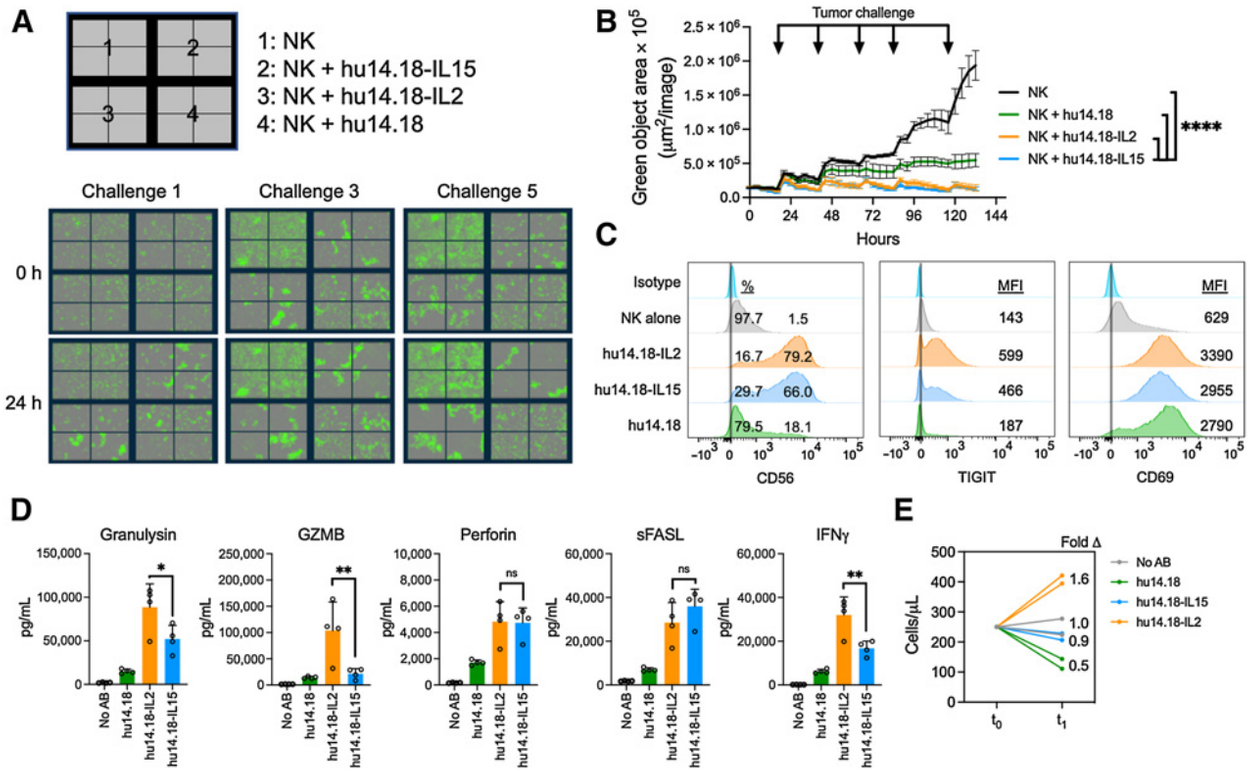

Figure 2.

NK cells maintain their cytolytic capacity with ICs during tumor rechallenge. **A,** Confluence of IMR-5-GFP cells during rechallenge experiment. **B,** Quantification of tumor cell confluence across all testing conditions over time; one-way ANOVA, ****, $P < 0.0001$. **C,** Flow cytometric analysis of CD56 (%), TIGIT (MFI), and CD69 (MFI) expressions in NK cells after the fifth tumor rechallenge. **D,** Cytokine levels in the culture supernatant after the fifth rechallenge; one-way ANOVA, *, $P < 0.05$; **, $P < 0.01$; ****, $P < 0.0001$. **E,** Expansion curves comparing cell numbers on days 0 (t_0) and 6 (t_1) of tumor rechallenge. One of two experimental replicates using two different donors is shown.

thirds of mice engrafted with SJNBL012407_X1 (**Fig. 3C–F**). In mice bearing SJNBL046_X, all except for one mouse in the hu14.18-IL15 arm had residual tumor (**Fig. 3G–I**). Mice receiving chemotherapy with ICs had less residual tumor burden in both models than animals in the chemotherapy arm. No differences in efficacy were noted comparing the three ICs. Most treated tumors at the end of the study retained high levels of GD2 expression (**Fig. 3F** and **I**), potentially rendering them sensitive to additional courses with chemotherapy and ICs. Altogether, these findings mirror the results from our *in vitro* studies, suggesting that the newly developed ICs have equivalent ADCC as hu14.18-IL2 in T-cell–deficient systems where NK cells serve as the sole effector cell population.

Hu14.18-IL15 and -IL21 outperform hu14.18-IL2 in immunocompetent models of orthotopic neuroblastoma

To compare the efficacy of all three ICs in an immunocompetent neuroblastoma mouse model, we implanted *MYCN*-WT GD2^{high} NXS-2-ffLUC cells into A/J mice and started treatment with ICs when animals established a defined tumor signal in the para-adrenal region on BLI (**Fig. 4A** and **B**). Using longitudinal BLI, we found that 3/7 (43%) mice treated with hu14.18-IL2 had a decline in BLI signals to near background levels by day 30 post tumor implantation compared with 5/7 (71%) treated with hu14.18-IL15 and 7/8 (88%) treated with hu14.18-IL21 (**Fig. 4C** and **D**). Corresponding tumor weights were also significantly smaller after treatment with the new ICs compared with vehicle or hu14.18-IL2 (**Fig. 4E**). As noted in our previous experiments (**Fig. 3F** and **I**), GD2 expression again remained high in residual tumor cells, suggesting that animals may benefit from additional doses of ICs (**Fig. 4F**). Furthermore, we found extended survival in animals that had received hu14.18-IL15 (**Fig. 4G** and **H**). Among the nine animals that survived beyond day 100, four were treated with hu14.18-IL15 and remained tumor-free. Animals that died before day 100 succumbed due to large tumor burden or small tumors invading the adjacent aorta leading to bleeding and death (**Fig. 4I**). Our findings demonstrate that hu14.18-IL15 and -IL21 outperformed hu14.18-IL2 in an immunocompetent host by controlling tumor growth within an early time window after IC administration, leading to long-term survival beyond 100 days in treated mice. Our results suggested that immune cells other than NK cells may influence the therapeutic efficacy of ICs. Thus, to further elucidate the contribution of tumor-infiltrating immune cells, we next sought to analyze the TME using multi-color flow cytometry and scRNA-seq.

Hu14.18-IL2 increases the fraction of Tregs in the TME

We have shown that we can detect tumor-bound ICs at 48 hours after intravenous injection of one dose (Supplementary Fig. S3). We, therefore, analyzed immune infiltrates in NXS-2 tumors of treated A/J mice 48 hours after one intravenous dose of IC using multicolor flow cytometry. The largest fraction of tumor-infiltrating immune cells comprised F4/80$^+$ macrophages (74%) followed by NK (9%), CD4$^+$ T

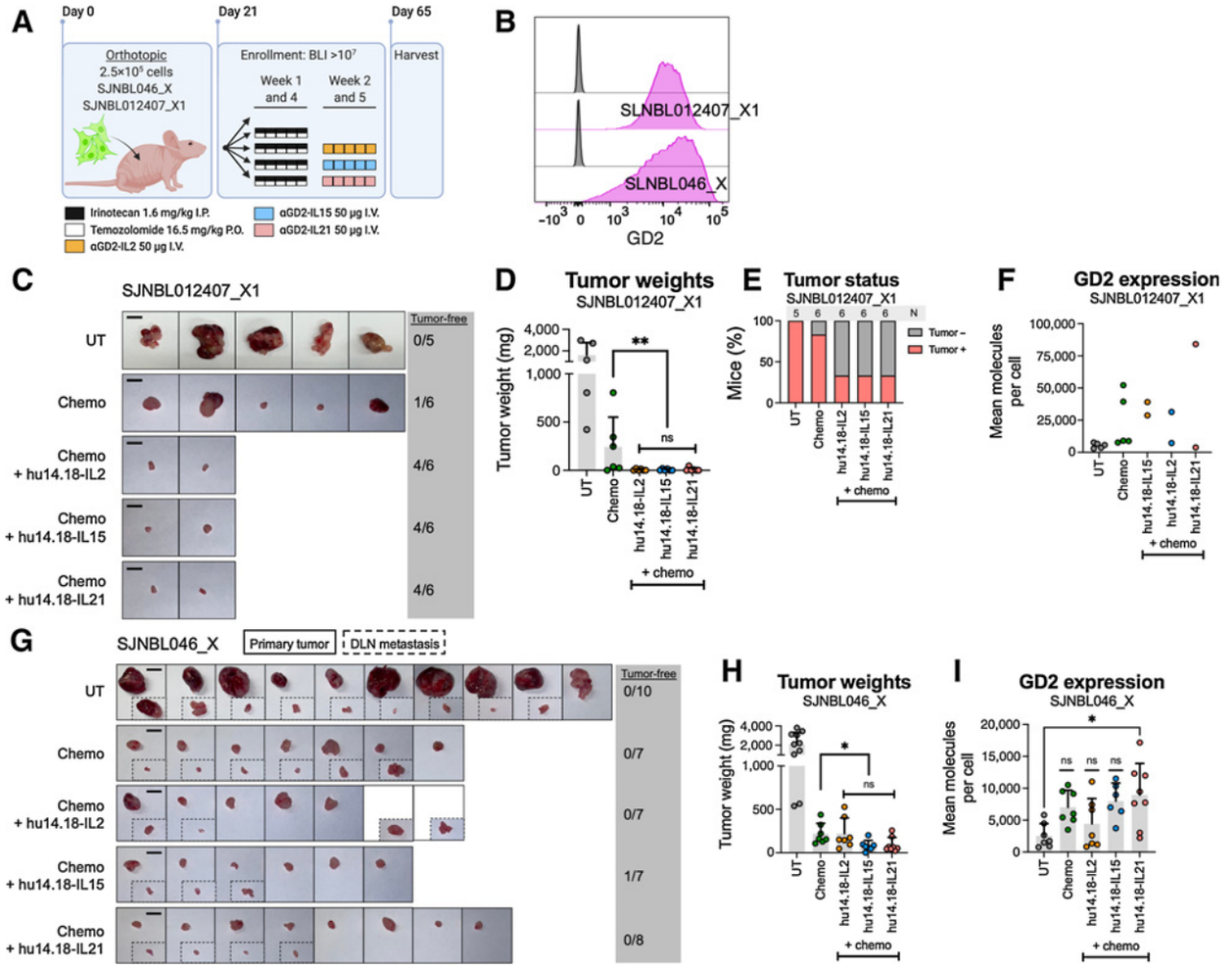

Figure 3.

ICs combined with chemotherapy suppress PDXs in T-cell–deficient mouse models. **A,** Description of the T-cell–deficient orthotopic PDX tumor model. **B,** GD2 expression levels in the two PDXs. *SJNBL012407_X1 model:* Appearance (**C**) and weights (**D**) on day 65 after tumor implantation; numbers of mice per group are shown as denominator on the right side of the images; scale, 1 cm; one-way ANOVA comparing ICs; The Mann–Whitney *U* test comparing chemotherapy versus ICs; **, $P < 0.01$; ns, nonsignificant. **E,** Numbers of tumor-free mice. **F,** GD2 expression of residual tumors. *SJNBL046_X model:* Appearance (**G**) and weights (**H**) on day 65 after tumor implantation; numbers of mice per group are shown as denominator on the right side of the images; scale, 1 cm; one-way ANOVA comparing ICs; the Mann–Whitney *U* test comparing chemotherapy versus ICs; **, $P < 0.001$; ns, nonsignificant. **I,** GD2 expression of residual tumors; one-way ANOVA with the Tukey *post hoc* test; *, $P < 0.05$; ns, nonsignificant.

(5%), and $CD8^+$ T cells (4%; Supplementary Fig. S5A). $CD8^+$ T cells exhibited 1.6-fold higher levels of perforin after hu14.18-IL21 treatment compared with no treatment, and a similar trend was noted in NK cells after administration of hu14.18-IL2 (Supplementary Fig. S5B). Most strikingly, the fraction (>1.7-fold) of Tregs was significantly elevated in animals treated with hu14.18-IL2 compared with all other treatment groups (Supplementary Fig. S5C), approximating 50% versus 30% of $CD4^+$ T cells, respectively. To extend these observations, we next conducted scRNA-seq of tumor-infiltrating leukocytes.

Hu14.18-IL15 increases M1-like TAMs and limit polymorphonuclear/granulocytic myeloid-derived suppressor cells in the TME

Three tumor-bearing animals per group were treated and after 48 hours, we dissociated the para-adrenal tumors, generated single-cell suspensions, and obtained 10^6 pooled cells from all animals for each group. These samples were further enriched for $CD45^+$ tumor-infiltrating leukocytes, and their transcriptomes were captured using the droplet-based 10X Genomics platform. After quality control and filtering, we obtained a total of 23,209 single-cell transcriptomes that comprised even proportions from each IC treatment group but contained fewer cells from control animals (**Fig. 5A**). We used *Ptprc* to distinguish immune cells from tumor cells (**Fig. 5B**). We found that roughly 50% of the samples accounted for immune cells in the IC groups, however, proportionally more leukocytes were derived from control animals, altogether yielding comparable total immune cell numbers (**Fig. 5C**; Supplementary Fig. S6). To define the main subsets of tumor-infiltrating leukocytes, we performed graph-based unsupervised clustering of *Ptprc*-expressing cells and used conventional markers to define T (*Cd3e*, *Cd8a*, *Cd4*), NK (*Ncr1*), B (*Ms4a1*), and dendritic cells (DC; *Siglech*), polymorphonuclear/granulocytic

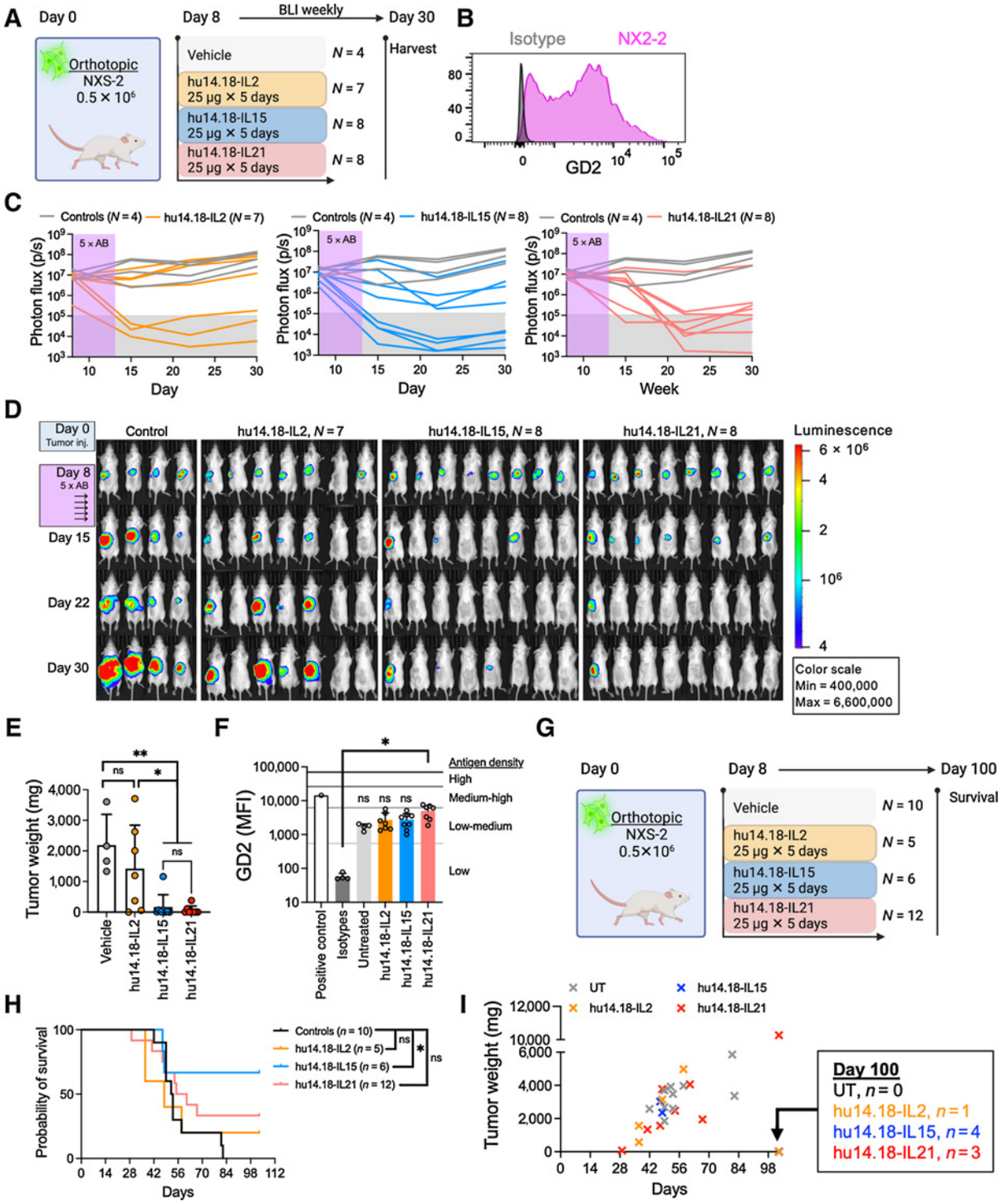

Figure 4.

New ICs outperform hu14.18-IL2 in an immunocompetent model of orthotopic neuroblastoma. **A,** Schema of model for tumor-regression study. **B,** GD2 expression levels in NXS-2-GD2^{high} cells. **C,** BLI tumor signal in different experimental groups over time. The gray area indicates the range of background signals. **D,** Corresponding images with normalized BLI signals from (**C**). **E,** Tumor weights on day 30 after orthotopic tumor implantation; the Kruskal–Wallis test with the Dunn *post hoc* test; *, $P < 0.05$; **, $P < 0.01$. **F,** GD2 levels in residual tumors on day 30 after implantation; one-way ANOVA with the Tukey *post hoc* test; *, $P < 0.05$; ns, nonsignificant. **G,** Schema of tumor model for survival study. **H,** Survival curves of mice; log-rank test; *, $P < 0.05$; ns, nonsignificant. **I,** Tumor size plotted against the day of death. Simple linear regression shown for significant correlations. UT: $r^2 = 0.41$, $P < 0.05$; hu14.18-IL15 $r^2 = 0.98$, $P = 0.0001$. One of three replicates is shown for the efficacy studies and one of two replicates for the survival study.

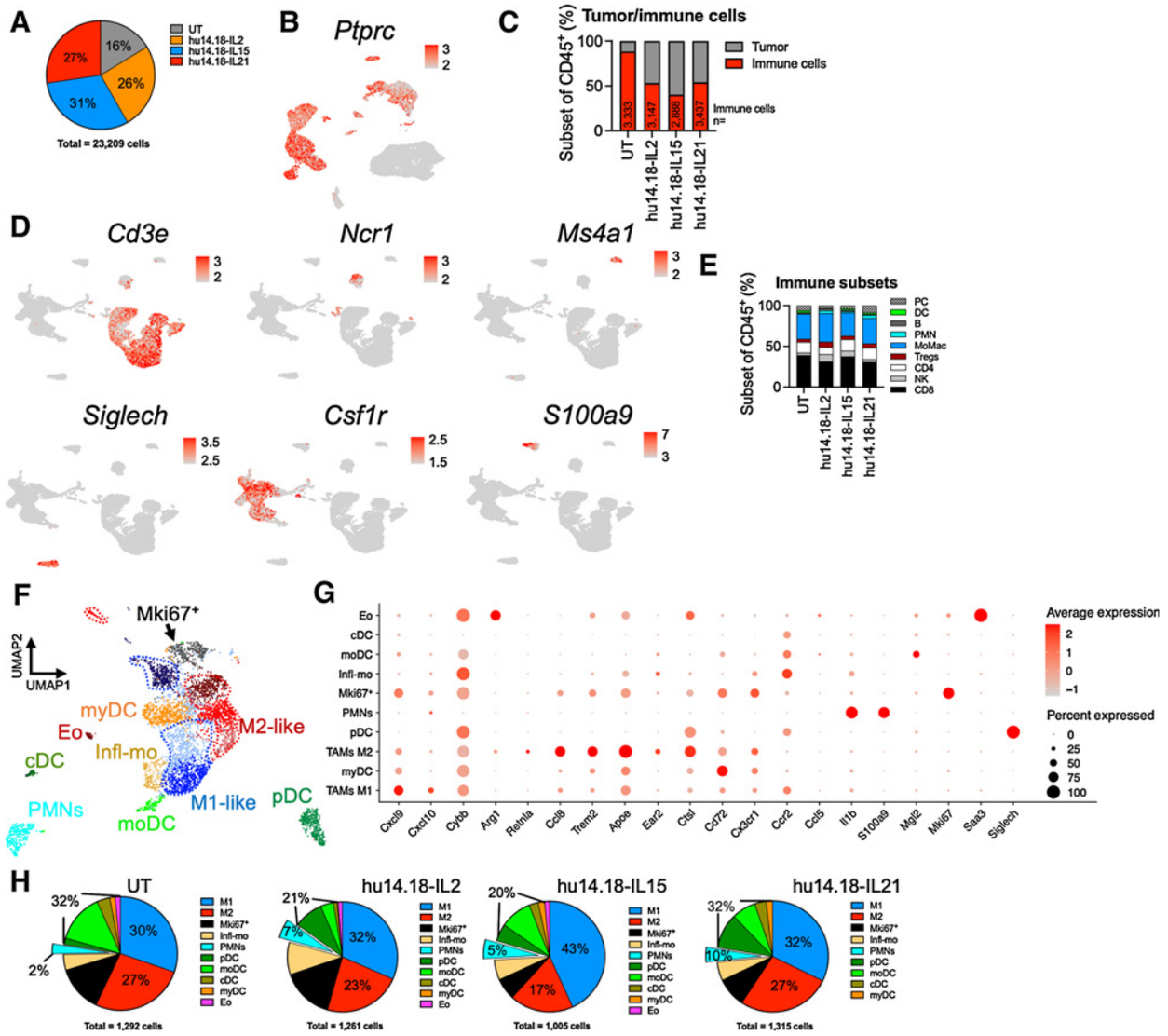

Figure 5.

Hu14.18-IL15 remodels the myeloid compartment toward an M1-biased TME of NSX-2–bearing A/J mice. **A,** Proportions of captured immune cells as per the treatment group. **B,** Separation of *Ptprc*-expressing immune cells from tumor cells. **C,** Percentages of *Ptprc*-positive and -negative cells in each therapy group. **D,** Feature plots with expression levels of selected genes among *Ptprc*-positive and reclustered cells. **E,** Quantification of immune cell subsets. PC, plasma cells; DC, dendritic cells; PMN, polymorphonuclear/granulocytic cells; MoMac, monocytes/macrophages; Tregs, T regulatory cells; NK, natural killer cells. **F,** UMAP plots showing 17 myeloid clusters with grouped annotations. **G,** Dot plot with marker genes across major myeloid clusters from (**E**). The dot size indicates the percentage of expressing cells, whereas the color-code represents the z-score normalized expression levels. **H,** Pie chart of myeloid subgroups separated by the treatment group.

(PMNs; *S100a9*), and macrophages/monocytes (*Csf1r*; **Fig. 5D**; Supplementary Figs. S7 and S8). Quantification of these subsets showed that CD8$^+$ T cells and macrophages/monocytes comprised the largest populations of immune cells (**Fig. 5E**), which is consistent with our findings from the multi-color flow cytometry analysis (Supplementary Fig. S5A).

Next, we performed separate analyses for myeloid (i.e., PMNs, DCs, monocytes, and macrophages) and lymphoid (i.e., T and NK cells) cell populations. A total of 17 cell clusters were defined by unsupervised clustering of the myeloid compartment (**Fig. 5F**), of which we excluded two clusters that contained predominantly ribosomal RNA and lacked lineage-defining genes (total of 170 cells, <4%). On the basis of gene signatures, we manually annotated each cluster and grouped them into M1-like (pro-inflammatory and cytotoxic) and M2-like (anti-inflammatory) tumor-associated macrophages (TAM), Mki67$^+$ myeloid cells, inflammatory monocytes, PMN-MDSCs (myeloid-derived–suppressor cells), classic DCs, monocyte-derived DCs, myeloid DCs, plasmacytoid DCs, and eosinophils (**Fig. 5G**; Supplementary Table S1). The M1-like clusters were characterized by high levels of the chemokines *Cxcl9* and *Cxcl10*. The M2-like clusters exhibited upregulation of *Arg1*, *Retlna*, *Ccl8*, and *Cxcr1*. Differentially expressed genes in PMN-MDSCs included *S100a8/9*, *Cxcl2*, *Cxcr2*, *Trem2*, and *Il1b*. Compared with untreated controls and hu14.18-IL2 and -IL21 treatment, animals receiving IL15 conjugated antibody had a

marked increase in *Cxcl9*- and *Cxcl10*-expressing M1-like TAMs (43% vs. ∼30%; Supplementary Table S2) in the TME, though measurement of the precise cell abundance should be interpreted in the context of the technical limitations of scRNA-seq. Both chemokines are known to regulate the recruitment of *Cxcr3*-expressing stem-like $CD8^+$ T cells to the TME and correlate with positive clinical responses to immune checkpoint blockade therapy (22–24). Furthermore, emerging data have demonstrated that M2-biased TMEs are associated with a poorer outcome in neuroblastoma (Supplementary Fig. S9; refs. 25, 26). Comparing the three ICs, we also noted a trend toward fewer *Cxcl2*-expressing PMN-MDSCs in mice treated with hu14.18-IL15 (5% vs. 7 and 10%; **Fig. 5H**). CXCL2 plays an essential role in suppressing the effector function of antigen-specific tumor-infiltrating lymphocytes, thereby countering responses to immunotherapy (27). Taken together, our findings demonstrate that ICs substantially alter the composition of the immune cell infiltrate in the TME. Hu14.18-IL15 caused a selective expansion of M1-like TAMs and led to the recruitment of fewer PMN-MDSCs. These findings are consistent with superior ADCC and survival in mice treated with hu14.18-IL15 compared with the other therapy groups.

ICs decrease the number of exhausted cytotoxic T cells in the TME

The same analytical approach that was applied to the myeloid compartment was used to interrogate the single-cell transcriptome of T and NK cells using. Unsupervised clustering revealed 20 independent cell clusters (**Fig. 6A**). On the basis of canonical genetic signatures (Supplementary Table S3), we assigned annotations manually. Tregs were identified by the expression of the transcription factors *Ikzf2* and *Foxp3* and NK cells by *Ncr1*. T_{cm} cells expressed high levels of *Il7r* and *Tcf7* but lacked differential expression of genes associated with effector function (28). A small subset of cells was characterized as tissue-resident memory (T_{RM}) cells based on the high expression of *Ly6c1/2*, *Cd69*, and *Cxcr6* (29). The cluster containing exhausted CD8 T cells was marked by enriched genes encoding chemokines (e.g., *Ccl3*, *Ccl4*), cytokines (e.g., *Ifng*), cytotoxic molecules (e.g., *Prf1*), and markers and transcription factors associated with functional exhaustion such as *Havcr2* and *Tox* (30, 31). Finally, two large clusters were identified as proliferating lymphocytes and $CD8^+$ cytokine secreters/responders. Comparing the different treatment groups (**Fig. 6B**; Supplementary Fig. S10), we found that ICs significantly decreased the numbers of exhausted $CD8^+$ T cells in the TME compared with vehicle-treated controls (Supplementary Table S4). Furthermore, we noted an expansion of NK cells with hu14.18-IL2 but found larger proportions of $CD8^+$ cytokine secreters/responders with hu14.18-IL15 and -IL21.

Next, we merged all clusters into 6 distinct subgroups based on cell type-specific genes (**Fig. 6C–E**). We then compared the proportions of the main cell populations across the treatment groups. Our scRNA-seq analysis corroborated previous flow cytometry findings (**Fig. 6C**), demonstrating almost twice as many Tregs with hu14.18-IL2 than with the other ICs (**Fig. 6F**). CD8 T cells were evenly represented across all four therapy groups; however, significantly elevated proportions of NK cells were associated with hu14.18-IL2 (**Fig. 6G–H**). Curiously, when we compared the fractions of proliferating cells within each cell type, we noted higher percentages of Mki67-expressing CD8 T and NK cells with hu14.18-IL2 but no difference among Tregs (**Fig. 6I**). This suggests that hu14.18-IL2 increases NK cell proportions through proliferative expansion, whereas Tregs may increase through recruitment to the TME.

To illuminate the transcriptional changes across the therapy groups, we performed separate differential gene expression analyses in $CD8^+$ T cells and NK cells comparing ICs with untreated controls (Supplementary Fig. S11). The transcriptional changes in $CD8^+$ T cells indicated that the cells undertake preparative measures for cytotoxic activity. For example, several mitochondrial genes (e.g., *Uqcr11*, *Atp5g*) were upregulated to increase energy generation. The expression of cathepsins was induced, possibly to process pro-granzymes into proteolytically active forms (32). Genes that protect against oxidative stress were likewise upregulated (**Fig. 6J**; ref. 33). Similarly, NK cells induced the expression of *Txn1*, *Prdx1*, *Cyba* (protective of oxidative stress), and cathepsins upon IC treatment. Comparisons between the IC groups showed very few transcriptomic differences in both $CD8^+$ T and NK cells. Hu14.18-IL15 and -IL21 had slightly higher levels of *Prf1* (1.2- and 1.4-fold increase) compared with hu14.18-IL2, respectively. Altogether, our data showed that treatment with ICs can increase the number of cytokine-secreting T cells and decrease the fraction of exhausted cytotoxic T cells in the TME most likely by converting them into functionally intact cells. Quantification of the cellular subsets also revealed that hu14.18-IL2 induced the proliferation of NK cells and recruited immune-suppressive Tregs to the TME. These cellular changes, including the shifts in the myeloid compartment toward a pro-immune environment, may contribute to superior ADCC induced by hu14.18-IL15 compared with the other two ICs.

Discussion

In the present study, we demonstrate that hu14.18-IL15 and hu14.18-IL21 exhibit robust preclinical activity against neuroblastoma and can remodel the TME, potentially overcoming immunosuppressive mechanisms. We and others previously demonstrated that precomplexed IL15/IL15Rα can induce impressive responses in humanized aggressive orthotopic neuroblastoma models (10, 11). However, because most patients experience significant systemic side effects with the administration of IL15 or IL15/IL15Rα complexes, more localized delivery strategies may be beneficial (34–36). We designed new ICs linking two other γ_c cytokines, IL15 and IL21, to hu14.18 and compared their ADCC with that of hu14.18-IL2.

Although it has been known that IL2 stimulates Tregs at lower doses (37, 38), IL15 and IL21 primarily act on $CD8^+$ T cells and NK cells (9), which renders them attractive alternative adjunct agents for immunotherapy. Aside from expanding $CD8^+$ T cells, we found that hu14.18-IL15 also acted on the myeloid compartment by decreasing the recruitment of MDSCs to the TME and increasing pro-immune M1 TAMs. These changes occurred with the added benefit of limiting the numbers of Tregs when compared with hu14.18-IL2. These cooperative effects can enhance the recruitment of cytotoxic T and NK cells and inhibit tumor angiogenesis via the CXCL9/CXCL10 axis, two chemokines that we found to be highly expressed in M1 TAMs (22). CCL3 and its paralogue CCL4 (also known as MIP-1α and MIP-1β), differentially expressed by $CD8^+$ T cells in our dataset, have diverse regulatory roles in the TME (39). As such, they can complement a pro-inflammatory response via the recruitment of antigen-primed DC to the TME to induce tumor rejection (40, 41) or by attracting $CD8^+$ T cells and macrophages to the primary tumor site to elicit cytotoxicity (42). Interestingly, we found equivalent ADCC between hu14.18-IL2 and hu14.18-IL15 in NK cell-based experimental *in vitro* systems and T-cell–deficient PDX models with NK cells as effector cells. These observations led us to believe that immune-suppressive mechanisms mediated by MDSCs and Tregs and

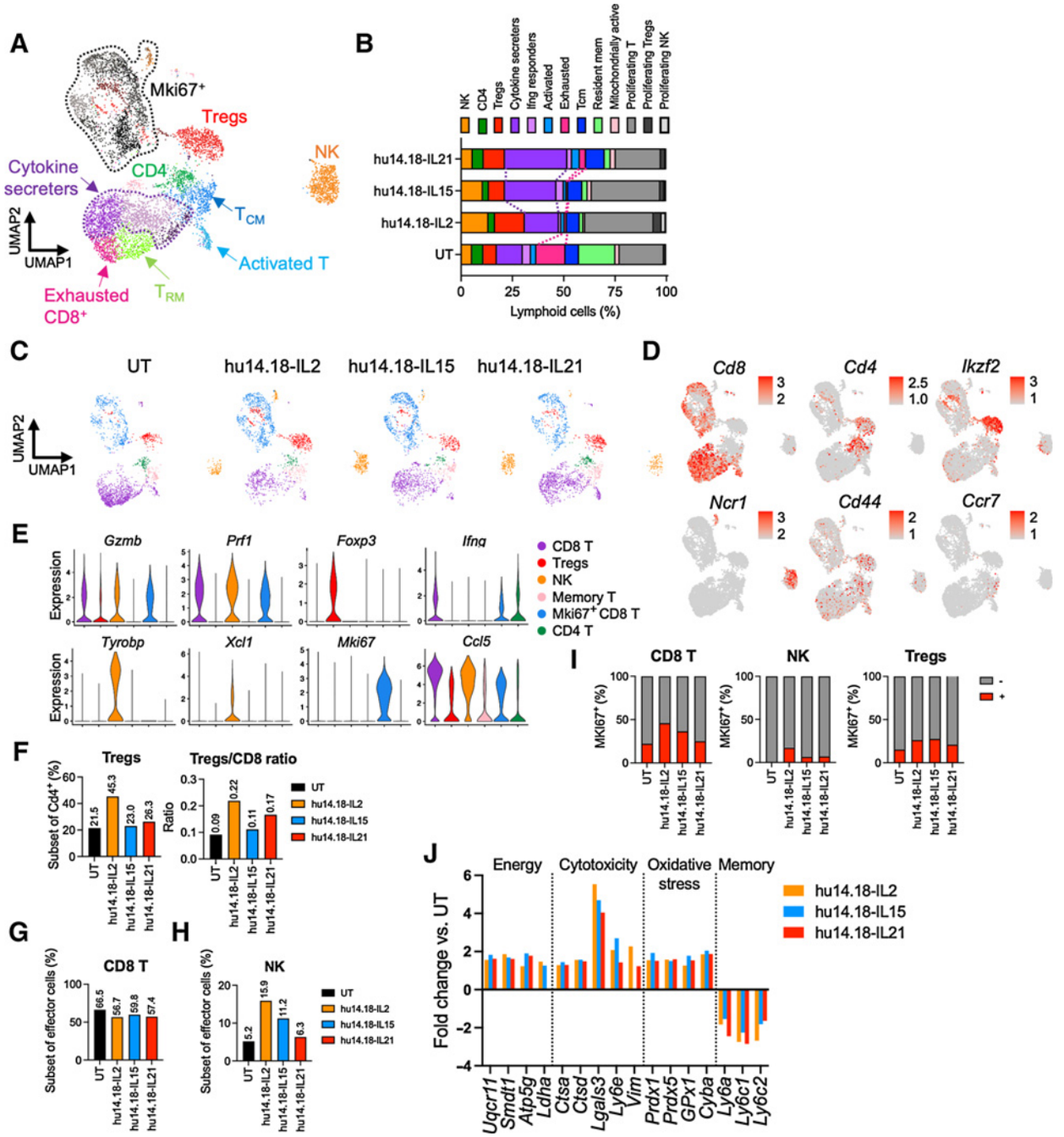

Figure 6.

ICs reduce the proportions of exhausted CD8$^+$ T cells in the TME of NSX-2–bearing A/J mice. **A,** UMAP plot of lymphoid cells. **B,** Proportions of lymphoid subsets in each group (some of which are connected by dashed lines across several groups). **C,** UMAP plots of lymphoid clusters merged into 6 main subsets. **D,** UMAP plots showing characteristic genes for each subset from (**C**). **E,** Violin plot of genes associated with cell function, activation, and cytotoxicity. **F,** Proportions of Tregs (left) and Treg/CD8 ratios (right). Percentages of CD8 T cells (**G**) and NK cells (**H**) as a fraction of all effector cells. **I,** Fraction of proliferating lymphocytes. **J,** Differential expression of selected genes that are functionally grouped comparing ICs versus untreated controls.

pro-immune effects executed by M1 TAMs and CD8$^+$ T cells in the TME were dominating factors in driving ADCC response in our study. So-called cytokine "muteins" with differential receptor affinities may be useful for the design of future ICs and allow a more selected engagement of desired effector subsets (43). Our work also emphasizes the need to use immune-competent syngeneic murine models complimentary to T-cell–deficient humanized tumor models for preclinical studies.

Among the causes of immunotherapy failure, antigen escape is a well-known mechanism after adoptive cellular therapies (44) and mAb treatment (45–47). Although the emergence of GD2-negative relapses

after monoclonal anti-GD2 antibody therapy has been reported in the clinic (48–50), it is unknown how many patients recur due to antigen loss. Interestingly, in neither of our *in vivo* model systems did we find substantial antigen loss in residual tumors post antibody administration. The measured GD2 expression approximated levels exhibited by the positive control. Thus, it is possible that repeated dosing of ICs could be therapeutically exploited given that NK cells maintain their cytolytic capacity during tumor rechallenge and the relative stability of GD2 expression on neuroblastoma cells.

Given the timing of our scRNA-seq analysis, we acknowledge that our mechanistic findings represent early changes and that analysis at later time points may be needed to illuminate the secondary and tertiary immunologic shifts in the TME upon treatment with ICs. Though cross-reactive between human and mice, one limitation of our ICs is possible immunogenicity of human cytokines in immunocompetent mice when given as repeated dosing cycles.

It is important to acknowledge that proteolytic cleavage of the cytokines can contribute to the occurrence of systemic toxicities as reported previously with hu14.18-IL2 (7). Therefore, it may be anticipated that patients can develop IL-15–related dose-limiting toxicities (e.g., hypotension, thrombocytopenia, and elevation of AST and ALT) during phase I dose-escalation studies (34). Our binding and distribution studies in mice showed that all three ICs were detected on tumor cells derived from the tumor tissue and in the serum at 48 hours (Supplementary Fig. S3). However, the levels of each cytokine were different in tumor tissue and serum, with IL2 being low on the tumor cells but elevated in the circulation, IL21 elevated in both locations, and IL15 being high on the tumor cells but low systemically. These differences corroborate the improved ADCC with hu14.18-IL15 and -IL21 compared with hu14.18-IL2 and could indicate differences in systemic exposures upon translation, which requires future confirmation in non-human primates and/or humans.

In summary, our study demonstrates that IL15 and IL21 are potent adjunct agents for the generation of ICs. Our work highlights that iterative preclinical testing of immunotherapies requires the use of immunocompetent models to emulate the complex immunologic interactions in the TME and gain accurate insights into mechanisms mediating preclinical responses. Our promising results require confirmation in the clinical context. Given the robust preclinical activity of hu14.18-IL15, we have identified an efficacious IC for further consideration for clinical testing in patients with GD2-expressing neuroblastoma. Additional testing in other preclinical models of GD2-expressing pediatric tumors such as osteosarcoma is also warranted.

Authors' Disclosures

R. Nguyen reports grants from the Department of Defense and other support from the NIH intramural research program, NCI during the conduct of the study. M. Sun reports grants from Government-National Cancer Institute during the conduct of the study. C.J. Thiele reports grants from Department of Defense during the conduct of the study. No disclosures were reported by the other authors.

Authors' Contributions

R. Nguyen: Conceptualization, resources, data curation, formal analysis, funding acquisition, validation, investigation, visualization, methodology, writing–original draft, writing–review and editing. **X. Zhang:** Formal analysis, writing–review and editing. **M. Sun:** Data curation, writing–review and editing. **S. Abbas:** Formal analysis, writing–review and editing. **C. Seibert:** Data curation, writing–review and editing. **M.C. Kelly:** Conceptualization, writing–review and editing. **J.F. Shern:** Formal analysis, writing–review and editing. **C.J. Thiele:** Formal analysis, writing–review and editing.

Acknowledgments

This study was supported by the Department of Defense Peer Reviewed Cancer Research Program (CA191207 to R. Nguyen) and the intramural research program of the National Institutes of Health (all authors). We want to thank the NCI CCR Animal Resource Program/NCI Biological Testing Branch (Dr. M. Custer and Kathy Divi) for providing mice for our experiments, the NIH CC Blood bank (Thomas Lewis) for providing healthy donor blood cells, the Biological Resources Branch at the Frederick National Laboratory for giving us cytokines and hu14.18-IL2, Drs. N. Taylor, Z. Liu, J. Gulley, and D. Cervi for reviewing the article and giving us thoughtful suggestions, Dr. A. Mendoza for his assistance with animal regulatory work, Dr. D. Arroyo for his scientific input, and the Children's Solid Tumor Network for providing PDX lines for our studies. The CCR Single Cell Analysis Facility was funded by FNLCR contract 75N91019D00024. Sequencing was performed in conjunction with the CCR Genomics Core. This work used the computational resources of the NIH HPC Biowulf cluster (http://hpc.nih.gov). Some figures were generated with Biorender.com.

The costs of publication of this article were defrayed in part by the payment of page charges. This article must therefore be hereby marked *advertisement* in accordance with 18 U.S.C. Section 1734 solely to indicate this fact.

Note

Supplementary data for this article are available at Clinical Cancer Research Online (http://clincancerres.aacrjournals.org/).

Received March 5, 2022; revised May 18, 2022; accepted July 6, 2022; published first July 8, 2022.

References

1. Yu AL, Gilman AL, Ozkaynak MF, London WB, Kreissman SG, Chen HX, et al. Anti-GD2 antibody with GM-CSF, interleukin-2, and isotretinoin for neuroblastoma. N Engl J Med 2010;363:1324–34.
2. Yu AL, Gilman AL, Ozkaynak MF, Naranjo A, Diccianni MB, Gan J, et al. Long-term follow-up of a phase III study of ch14.18 (Dinutuximab) + cytokine immunotherapy in children with high-risk neuroblastoma: COG study ANBL0032. Clin Cancer Res 2021;27:2179–89.
3. Neal ZC, Yang JC, Rakhmilevich AL, Buhtoiarov IN, Lum HE, Imboden M, et al. Enhanced activity of hu14.18-IL2 immunocytokine against murine NXS2 neuroblastoma when combined with interleukin 2 therapy. Clin Cancer Res 2004;10:4839–47.
4. Yang RK, Kalogriopoulos NA, Rakhmilevich AL, Ranheim EA, Seo S, Kim K, et al. Intratumoral treatment of smaller mouse neuroblastoma tumors with a recombinant protein consisting of IL-2 linked to the hu14.18 antibody increases intratumoral $CD8^+$ T and NK cells and improves survival. Cancer Immunol Immunother 2013;62:1303–13.
5. Shusterman S, London WB, Gillies SD, Hank JA, Voss SD, Seeger RC, et al. Antitumor activity of hu14.18-IL2 in patients with relapsed/refractory neuroblastoma: a Children's Oncology Group (COG) phase II study. J Clin Oncol 2010;28:4969–75.
6. Shusterman S, Naranjo A, Van Ryn C, Hank JA, Parisi MT, Shulkin BL, et al. Antitumor activity and tolerability of hu14.18-IL2 with GMCSF and isotretinoin in recurrent or refractory neuroblastoma: a children's oncology group phase II study. Clin Cancer Res 2019;25:6044–51.
7. Osenga KL, Hank JA, Albertini MR, Gan J, Sternberg AG, Eickhoff J, et al. A phase I clinical trial of the hu14.18-IL2 (EMD 273063) as a treatment for children with refractory or recurrent neuroblastoma and melanoma: a study of the children's oncology group. Clin Cancer Res 2006;12:1750–9.
8. Ladenstein R, Potschger U, Valteau-Couanet D, Luksch R, Castel V, Yaniv I, et al. Interleukin 2 with anti-GD2 antibody ch14.18/CHO (dinutuximab beta) in patients with high-risk neuroblastoma (HR-NBL1/SIOPEN): a multicentre, randomised, phase 3 trial. Lancet Oncol 2018;19:1617–29.
9. Leonard WJ, Lin JX, O'Shea JJ. The gammac family of cytokines: basic biology to therapeutic ramifications. Immunity 2019;50:832–50.
10. Nguyen R, Moustaki A, Norrie JL, Brown S, Akers WJ, Shirinifard A, et al. Interleukin-15 enhances anti-GD2 antibody-mediated cytotoxicity in an orthotopic PDX model of neuroblastoma. Clin Cancer Res 2019;25:7554–64.
11. Chu Y, Nayyar G, Jiang S, Rosenblum JM, Soon-Shiong P, Safrit JT, et al. Combinatorial immunotherapy of N-803 (IL-15 superagonist) and dinutuximab

with *ex vivo* expanded natural killer cells significantly enhances *in vitro* cytotoxicity against GD2(+) pediatric solid tumors and *in vivo* survival of xenografted immunodeficient NSG mice. J Immunother Cancer 2021;9:e002267.
12. Hank JA, Surfus JE, Gan J, Ostendorf A, Gillies SD, Sondel PM. Determination of peak serum levels and immune response to the humanized anti-ganglioside antibody-interleukin-2 immunocytokine. In: Buolamwini JK, Adjei AA, editors. Novel anticancer drug protocols. Totowa, NJ: Humana Press; 2003. p. 123–31.
13. Nguyen R, Houston J, Chan WK, Finkelstein D, Dyer MA. The role of interleukin-2, all-trans retinoic acid, and natural killer cells: surveillance mechanisms in anti-GD2 antibody therapy in neuroblastoma. Cancer Immunol Immunother 2018;67:615–26.
14. Mody R, Naranjo A, Van Ryn C, Yu AL, London WB, Shulkin BL, et al. Irinotecan-temozolomide with temsirolimus or dinutuximab in children with refractory or relapsed neuroblastoma (COG ANBL1221): an open-label, randomised, phase 2 trial. Lancet Oncol 2017;18:946–57.
15. Mody R, Yu AL, Naranjo A, Zhang FF, London WB, Shulkin BL, et al. Irinotecan, temozolomide, and dinutuximab with GM-CSF in children with refractory or relapsed neuroblastoma: a report from the children's oncology group. J Clin Oncol 2020;38:2160–9.
16. Li N, Nguyen R, Thiele CJ, Ho M. Preclinical testing of chimeric antigen receptor T cells in neuroblastoma mouse models. STAR Protoc 2021;2:100942.
17. Young MD, Behjati S. SoupX removes ambient RNA contamination from droplet-based single-cell RNA sequencing data. Gigascience 2020;9:giaa151.
18. Wolock SL, Lopez R, Klein AM. Scrublet: computational identification of cell doublets in single-cell transcriptomic data. Cell Syst 2019;8:281–91.
19. Stuart T, Butler A, Hoffman P, Hafemeister C, Papalexi E, Mauck WM, 3rd, et al. Comprehensive integration of single-cell data. Cell 2019;177:1888–902.
20. Imamura M, Shook D, Kamiya T, Shimasaki N, Chai SM, Coustan-Smith E, et al. Autonomous growth and increased cytotoxicity of natural killer cells expressing membrane-bound interleukin-15. Blood 2014;124:1081–8.
21. Albertini MR, Hank JA, Gadbaw B, Kostlevy J, Haldeman J, Schalch H, et al. Phase II trial of hu14.18-IL2 for patients with metastatic melanoma. Cancer Immunol Immunother 2012;61:2261–71.
22. Mikucki ME, Fisher DT, Matsuzaki J, Skitzki JJ, Gaulin NB, Muhitch JB, et al. Non-redundant requirement for CXCR3 signalling during tumoricidal T-cell trafficking across tumour vascular checkpoints. Nat Commun 2015;6:7458.
23. House IG, Savas P, Lai J, Chen AXY, Oliver AJ, Teo ZL, et al. Macrophage-derived CXCL9 and CXCL10 are required for antitumor immune responses following immune checkpoint blockade. Clin Cancer Res 2020;26:487–504.
24. Qu Y, Wen J, Thomas G, Yang W, Prior W, He W, et al. Baseline frequency of inflammatory Cxcl9-expressing tumor-associated macrophages predicts response to avelumab treatment. Cell Rep 2020;32:107873.
25. Liu D, Song L, Wei J, Courtney AN, Gao X, Marinova E, et al. IL-15 protects NKT cells from inhibition by tumor-associated macrophages and enhances antimetastatic activity. J Clin Invest 2012;122:2221–33.
26. Liu KX, Joshi S. "Re-educating" tumor associated macrophages as a novel immunotherapy strategy for neuroblastoma. Front Immunol. 2020;11:1947.
27. Sun L, Clavijo PE, Robbins Y, Patel P, Friedman J, Greene S, et al. Inhibiting myeloid-derived suppressor cell trafficking enhances T-cell immunotherapy. JCI Insight 2019;4:e126853.
28. Pais Ferreira D, Silva JG, Wyss T, Fuertes Marraco SA, Scarpellino L, Charmoy M, et al. Central memory CD8(+) T cells derive from stem-like Tcf7(hi) effector cells in the absence of cytotoxic differentiation. Immunity 2020;53:985–1000.
29. Stelma F, de Niet A, Sinnige MJ, van Dort KA, van Gisbergen K, Verheij J, et al. Human intrahepatic CD69$^+$ CD8$^+$ T cells have a tissue resident memory T-cell phenotype with reduced cytolytic capacity. Sci Rep 2017;7:6172.
30. Khan O, Giles JR, McDonald S, Manne S, Ngiow SF, Patel KP, et al. TOX transcriptionally and epigenetically programs CD8$^+$ T-cell exhaustion. Nature 2019;571:211–8.
31. Sakuishi K, Apetoh L, Sullivan JM, Blazar BR, Kuchroo VK, Anderson AC. Targeting Tim-3 and PD-1 pathways to reverse T-cell exhaustion and restore antitumor immunity. J Exp Med 2010;207:2187–94.
32. Burkhardt JK, Hester S, Lapham CK, Argon Y. The lytic granules of natural killer cells are dual-function organelles combining secretory and pre-lysosomal compartments. J Cell Biol 1990;111:2327–40.
33. Klopotowska M, Bajor M, Graczyk-Jarzynka A, Kraft A, Pilch Z, Zhylko A, et al. PRDX-1 supports the survival and antitumor activity of primary and CAR-modified NK cells under oxidative stress. Cancer Immunol Res 2022;10:228–44.
34. Conlon KC, Lugli E, Welles HC, Rosenberg SA, Fojo AT, Morris JC, et al. Redistribution, hyperproliferation, activation of natural killer cells and CD8 T cells, and cytokine production during first-in-human clinical trial of recombinant human interleukin-15 in patients with cancer. J Clin Oncol 2015;33:74–82.
35. Romee R, Cooley S, Berrien-Elliott MM, Westervelt P, Verneris MR, Wagner JE, et al. First-in-human phase 1 clinical study of the IL-15 superagonist complex ALT-803 to treat relapse after transplantation. Blood 2018;131:2515–27.
36. Wrangle JM, Velcheti V, Patel MR, Garrett-Mayer E, Hill EG, Ravenel JG, et al. ALT-803, an IL-15 superagonist, in combination with nivolumab in patients with metastatic non–small cell lung cancer: a non-randomised, open-label, phase 1b trial. Lancet Oncol 2018;19:694–704.
37. Kennedy-Nasser AA, Ku S, Castillo-Caro P, Hazrat Y, Wu MF, Liu H, et al. Ultra low-dose IL-2 for GVHD prophylaxis after allogeneic hematopoietic stem cell transplantation mediates expansion of regulatory T cells without diminishing antiviral and antileukemic activity. Clin Cancer Res 2014;20:2215–25.
38. Rosenzwajg M, Churlaud G, Mallone R, Six A, Derian N, Chaara W, et al. Low-dose interleukin-2 fosters a dose-dependent regulatory T-cell tuned milieu in T1D patients. J Autoimmun 2015;58:48–58.
39. Cook DN, Smithies O, Strieter RM, Frelinger JA, Serody JS. CD8$^+$ T cells are a biologically relevant source of macrophage inflammatory protein-1α *in vivo*. J Immunol 1999;162:5423–8.
40. Allen F, Bobanga ID, Rauhe P, Barkauskas D, Teich N, Tong C, et al. CCL3 augments tumor rejection and enhances CD8(+) T-cell infiltration through NK and CD103(+) dendritic cell recruitment via IFNgamma. Oncoimmunology 2018;7:e1393598.
41. Spranger S, Bao R, Gajewski TF. Melanoma-intrinsic beta-catenin signalling prevents anti-tumour immunity. Nature 2015;523:231–5.
42. Castellino F, Huang AY, Altan-Bonnet G, Stoll S, Scheinecker C, Germain RN. Chemokines enhance immunity by guiding naive CD8$^+$ T cells to sites of CD4$^+$ T-cell–dendritic cell interaction. Nature 2006;440:890–5.
43. Silva DA, Yu S, Ulge UY, Spangler JB, Jude KM, Labao-Almeida C, et al. *De novo* design of potent and selective mimics of IL-2 and IL-15. Nature 2019;565:186–91.
44. Majzner RG, Mackall CL. Tumor antigen escape from CAR T-cell therapy. Cancer Discov 2018;8:1219–26.
45. Foran JM, Norton AJ, Micallef IN, Taussig DC, Amess JA, Rohatiner AZ, et al. Loss of CD20 expression following treatment with rituximab (chimaeric monoclonal anti-CD20): a retrospective cohort analysis. Br J Haematol 2001;114:881–3.
46. Pickartz T, Ringel F, Wedde M, Renz H, Klein A, von Neuhoff N, et al. Selection of B-cell chronic lymphocytic leukemia cell variants by therapy with anti-CD20 monoclonal antibody rituximab. Exp Hematol 2001;29:1410–6.
47. Jones JD, Hamilton BJ, Rigby WF. Rituximab mediates loss of CD19 on B cells in the absence of cell death. Arthritis Rheum 2012;64:3111–8.
48. Kramer K, Gerald WL, Kushner BH, Larson SM, Hameed M, Cheung NK. Disaloganglioside GD2 loss following monoclonal antibody therapy is rare in neuroblastoma. Med Pediatr Oncol 2001;36:194–6.
49. Schumacher-Kuckelkorn R, Volland R, Gradehandt A, Hero B, Simon T, Berthold F. Lack of immunocytological GD2 expression on neuroblastoma cells in bone marrow at diagnosis, during treatment, and at recurrence. Pediatr Blood Cancer 2017;64:46–56.
50. Mazot P, Cazes A, Dingli F, Degoutin J, Irinopoulou T, Boutterin MC, et al. Internalization and downregulation of the ALK receptor in neuroblastoma cell lines upon monoclonal antibodies treatment. PLoS ONE 2012;7:e33581.